Applied Surface Science 722 (2026) 165504

Contents lists available at ScienceDirect

Applied Surface Science

journal homepage: www.elsevier.com/locate/apsusc

Full Length Article

Rapid characterisation of millimetre-tall vertically aligned carbon nanotube arrays: growth optimisation by tuning the catalyst film thickness

Xinghai Zhao [a,*], Johannes Eduard Stubbe [a,b], Jin Chuen Kenneth Ho [a], Putu Andhita Dananjaya [c], Wen Siang Lew [c], Philippe Coquet [b,d], Beng Kang Tay [a,b,**]

[a] School of Electrical and Electronic Engineering, Nanyang Technological University, 639798, Singapore
[b] IRL3288 CINTRA (CNRS-NTU-THALES), Nanyang Technological University, Singapore 637553 Singapore
[c] School of Physical and Mathematical Sciences, Nanyang Technological University, 637371 Singapore
[d] Institut d'Electronique, Microélectronique et Nanotechnologie, CNRS, Univ. Lille F-59000 Lille, France

ARTICLE INFO

Keywords:
Carbon nanotubes
VACNT
Catalyst film thickness
Areal density
Growth tortuosity
Characterisation
Fourier component analysis

ABSTRACT

This study aims to establish a quick and sustainable approach for optimising the growth of millimetre-tall vertically aligned carbon nanotube (VACNT) arrays through simple catalyst tuning. To achieve this swiftly, a rapid and handy characterisation protocol is essential. Herein, we propose and validate such a method for the rapid characterisation of VACNTs, which concurrently improves upon the traditional weight-gain density calculation for VACNT arrays. We demonstrate the efficacy of this combined strategy by systematically investigating the influence of iron (Fe) catalyst film thickness (0.8–2.0 nm) on the microstructure and density of VACNT arrays synthesised via thermal chemical vapour deposition (TCVD). Catalyst morphology was characterised by atomic force microscopy (AFM), while transmission electron microscopy (TEM) provided nanotube diameter and wall-number distributions. Scanning electron microscopy (SEM) measured array height for areal density estimation, with Fourier component analysis of SEM cross-sections applied to correct height underestimations from tube tortuosity. It was observed that increasing Fe thickness enlarges and broadens catalyst particle distributions, enabling modest tuning of VACNT dimensions without compromising packing density. An optimum film thickness of ~1.1 nm was identified, maximising areal density at ~2×10^{10} CNTs cm^{-2}. The integrated imaging and analysis approach presented here offers a practical and efficient pathway for rapid VACNT microstructure control and density assessment, facilitating future optimisation cycles. Furthermore, a transition in growth mode was observed, which further confirms the decisive role of the catalyst film thickness.

1. Introduction

Carbon nanotubes (CNTs) are cylindrical nanostructures composed of carbon atoms, notable for their extraordinary electrical and mechanical properties, which sustain their diverse applications [1–7]. In electronics, high-aspect-ratio and millimetre-tall VACNTs show promise as potential replacements for metals in interconnects and interlayer vias within integrated circuits due to their ability to carry very high current densities [8,9]. However, as one-dimensional conductors, individual CNTs exhibit inherent quantum resistance. To achieve high conductivity comparable to metal, billions of CNTs must be densely packed in parallel, necessitating a high areal density for practical applications [10–14]. Apart from areal density, the diameter and number of walls in CNTs significantly influence the collective behaviour of VACNT arrays when used as bulk materials [15,16]. For instance, an increase in wall number can double electrical conductivity while halving thermal conductivity [17]. Additionally, CNT length has been shown to scale nearly linearly with electrical conductivity via the aspect ratio, making VACNT arrays attractive as lightweight, low-cost, conductive materials [15]. Consequently, the ability to tailor the structure of CNT arrays is a promising approach for optimising their functional properties, but it remains challenging. Some state-of-the-art iron-catalysed VACNT research regarding the used substrate, growth conditions and properties, characterisation method has been summarised in Table S1 for reference.

The precise characterisation of VACNT array properties is a critical enabler for their transition from laboratory prototypes to functional

* Coressponding author.
** Coressponding author at: School of Electrical and Electronic Engineering, Nanyang Technological University, 639798, Singapore.
E-mail addresses: xinghai.zhao@ntu.edu.sg (X. Zhao), ebktay@ntu.edu.sg (B.K. Tay).

https://doi.org/10.1016/j.apsusc.2025.165504
Received 22 September 2025; Received in revised form 26 November 2025; Accepted 4 December 2025
Available online 5 December 2025

devices. This necessity is acutely evident in the context of millimetre-tall VACNT arrays, which present a compelling material platform for a suite of advanced applications. Their high mechanical compliance and vast specific surface area are indispensable for crafting high-strength, lightweight composites [18]. Simultaneously, their exceptional axial thermal conductivity positions them as next-generation thermal interface materials for dissipating heat in high-power electronics [19]. Furthermore, their structural anisotropy and electrical conductance make them ideal candidates for use as vertical interconnects in three-dimensional integrated circuits [20]. The precise morphological control plays the pivotal role in realising these application potentials [6,21]. At the heart of this control lies the accurate measurement of CNT areal density, a fundamental property dictated by their nanoscale dimensions[22]. Existing techniques for areal density quantification, however, present significant trade-offs. Direct enumeration from scanning electron microscopy (SEM) images is statistically inconsistent [12], while liquid-induced compaction suffers from artefacts and procedural complexities [23]. Although the conventional weight-gain method, derived from the volumetric density of carbon [24], offers improved reliability, its accuracy is inherently compromised by variations in carbon mass density due to crystallinity and defect density [25]. Even novel approaches like synchrotron X-ray scattering are impractical for routine optimisation [26]. To bridge this methodological gap, we have refined the weight-gain methodology into a robust and accurate protocol.

Despite advancements in characterisation instrumentation and methods, some details of CNT growth mechanisms remain obscure [3,27,28]. VACNT arrays serve as a model system for investigating the relationship between microstructural parameters (e.g., diameter, wall number, conductivity, waviness) and macroscopic growth characteristics (e.g., height, density, growth rate, catalyst thickness). The role of the catalyst is particularly critical in determining the final structure of CNT forests [3]. A key strategy for controlling VACNT array structure involves engineering the catalyst, especially by adjusting the thickness of the catalytic metal film. In this work, catalyst thickness and growth time were the only variables manipulated to understand better how microstructural changes affect VACNT growth.

This work introduces an integrated characterisation and optimisation framework that leverages this improved density metric to correlate catalyst geometry with VACNT morphology rapidly. We systematically analyse the effects of Fe catalyst film thickness on nanoparticle evolution, CNT diameter, wall number, and ultimately, the achieved areal and volumetric densities. Moreover, we introduce straightforward image processing techniques to quantify critical, yet often overlooked, growth dynamics in tall arrays, such as density decay and collective tube tortuosity. By unifying cost-effective nanoscale imaging (SEM, AFM, TEM) with rigorous density validation, this methodology provides a rapid and practical feedback loop for VACNT quality assessment. It thereby establishes an efficient pathway for tailoring VACNT physical characteristics (diameter, wall number, and density) through precise catalyst engineering, directly addressing the stringent requirements of their target applications.

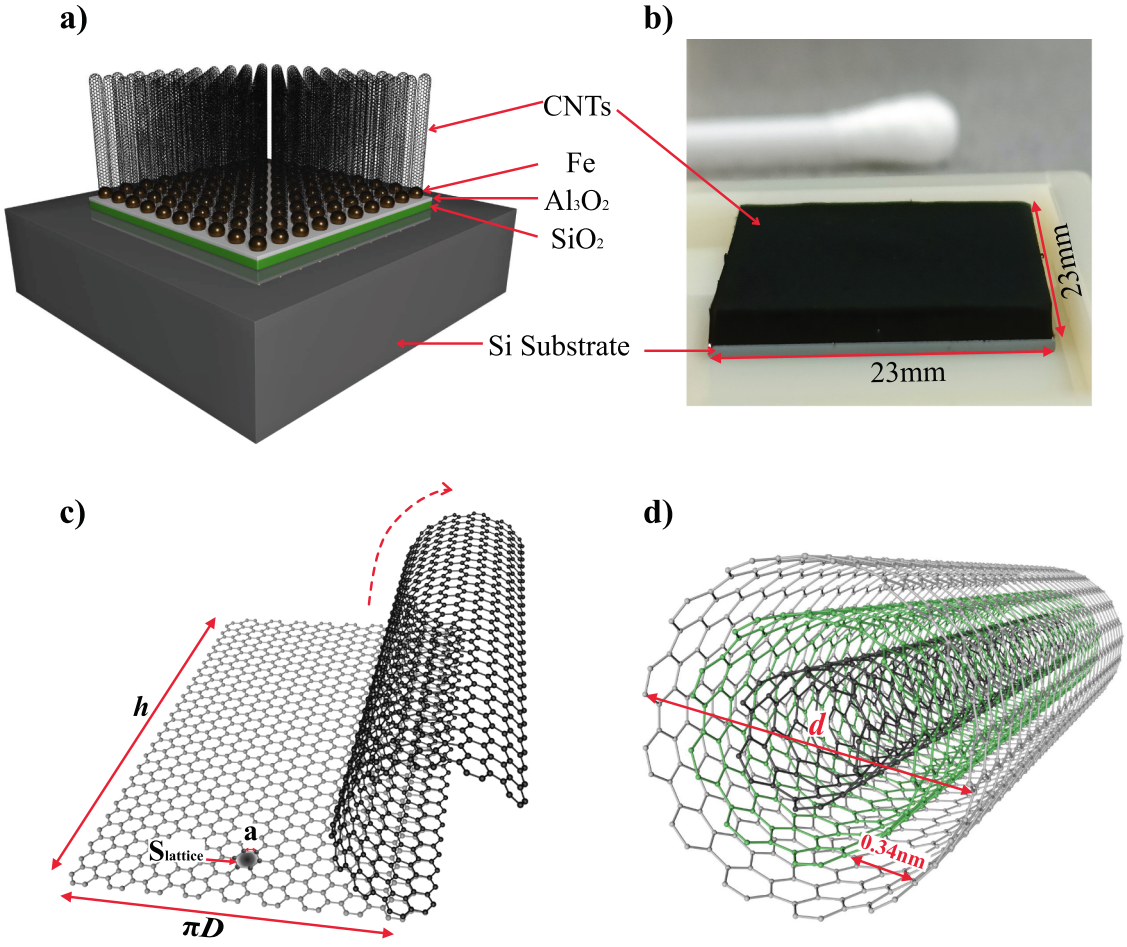

Fig. 1. VACNT growth. (a) Illustration of the layer structure of substrate for VACNT array growth, (b) image of a mm-height VACNT carpet grown on a 23 × 23 mm^2 silicon substrate using TCVD, schematic of (c) a schematic structure of "un-rolled" individual CNT and (d) a schematic structure of MWCNT.

2. Experimental and characterisation methods

2.1. Growth of VACNTs

In all experiments, the growth substrate consisted of Fe/Al_2O_3 deposited on thermally oxidised 4-inch silicon wafers using electron beam evaporation (Cello Ohmiker-60BL) at a deposition rate of 0.02 Å/s. As shown in Fig. 1(a), a 10-nm Al_2O_3 buffer layer was initially deposited onto silicon wafers pre-coated with a 200-nm thermally grown oxide layer. The Fe layers of varying thicknesses were then deposited onto the buffer layer using electron beam physical vapour deposition. The wafers were subsequently diced into 23 × 23 mm^2 square pieces. Multiple samples were prepared with Fe catalyst layers ranging from 0.8 to 2.0 nm to investigate the influence of catalyst thickness. VACNT arrays (Fig. 1b) were synthesised using a commercial TCVD system (FirstNano Easytube 3000) following a proprietary process. The furnace was preheated to 600 °C, after which the wafers were inserted into the chamber. Argon (Ar) and hydrogen (H_2) gases were introduced to anneal the samples for 5 min before the temperature was ramped to the growth temperature of 750 °C. During annealing, the Fe films coalesced into nanoparticles. Ethylene (C_2H_4) was then introduced as the carbon source, while trace amounts of water vapour (H_2O) were added via an Ar bubbler to promote CNT growth. Different array heights were achieved by varying the growth duration.

2.2. Structural and morphological characterisation

The height of the VACNT arrays was measured using a SEM (JEOL JSM-IT100). For each sample, measurements were taken at nine different locations to determine the average growth height. The detailed morphology and alignment of the VACNTs were further examined using a high-resolution field-emission SEM (Thermo Fisher Apreo S). For thickness and wall counting, CNTs were dispersed in ethanol and then observed using a high-resolution TEM (JEOL JEM-2100F). For each catalyst thickness (0.8 nm, 1.1 nm, 1.4 nm, 1.7 nm, and 2.0 nm), TEM measurements were averaged over 35–45 nanotubes to obtain representative values. The morphology of the iron catalyst nanoparticles was analysed using an atomic force microscope (AFM, Park NX10). The scanning parameters were fixed across all the samples to ensure a fair comparison could be made. The scan area of 0.5 × 0.5 μm^2 was used with 2048 pixels resolution in the *x-y* direction and a scan rate of 1.5 Hz. The AFM was operated under non-contact mode (NCM) using OMCL-AC160S AFM tips (radius of <10 nm) with optimised tip-sample distance and driving frequency of 298 kHz to obtain the best image quality while preserving both the sample surface and the AFM tip radius. The mass of the VACNT arrays was determined by weighing the silicon substrate before and after CNT growth using an electronic microbalance with a precision of 0.001 mg. The mass difference was used to calculate the areal density of the CNT array, incorporating the measured diameter, wall number, and growth height. In addition, Raman spectrum measurement has been used to confirm a good crystallinity of CNT structures, as shown in Fig. S1.

2.3. Density calculation method of the VACNTs

CNTs can be conceptualised as graphene sheets of sp2-bonded carbon atoms rolled up into seamless cylinders, as shown in Fig. 1(c). Multi-walled carbon nanotube (MWCNT) can be described as several graphite layers wrapped into a concentric seamless cylinder (Fig. 1d). The interlayer distance in an MWCNT is approximately that of graphite (0.34 nm) [29]. Therefore, the mass of a single MWCNT can be achieved by a simple calculation of the total carbon atoms. Subsequently, the areal density of MWCNT arrays can be reckoned by following the experimental procedures in Fig. S2.

We measure the average height, diameter, and number of walls of a subset of CNTs and then model the VACNT array based on these average properties. Consequently, all tubes will have the same mass m_{tube}. We refer to Eq. (1) below to find the areal density ρ_A:

$$\rho_v = \frac{M}{A} \tag{1}$$

$$\rho_A = \frac{N_{tube}}{A} = \frac{M}{Am_{tube}} \tag{2}$$

M is VACNT array mass, A is the substrate area. The mass of a single tube, m_{tube} is defined as:

$$m_{tube} = \frac{2\mathrm{m_c}S_{tube}}{\mathrm{S_{lattice}}} \tag{3}$$

where S_{tube} is the total surface area of an MWCNT, $\mathrm{m_c}$ is the mass of a carbon atom (1.994×10^{-19} g), and $\mathrm{S_{lattice}}$ is the surface area of a single hexagonal lattice. The formula aims to find the total number of carbon atoms in a tube and multiply it by the mass of carbon m_c. To find the number of carbon atoms, we first find $S_{tube,}$ where all walls contribute to its mass:

$$S_{tube} = \pi Dh \tag{4}$$

The interplanar spacing between walls is t. With an outer diameter of d, the total perimeter D with n number of walls that all contribute to the total mass can be found as:

$$D = \sum_{i=1}^{n} [d - 2t(i-1)] = nd - n(n-1)t \tag{5}$$

With the total surface area S_{tube} found, the number of hexagonal lattices can be found by dividing it by the hexagonal area $\mathrm{S_{lattice}}$:

$$\mathrm{S_{lattice}} = \frac{3\sqrt{3}\mathrm{a}^2}{2} \tag{6}$$

$$\rho_A = \frac{M}{Am_{tube}} = 0.413 \bullet \frac{\mathrm{a}^2}{\mathrm{m_c}} \bullet \frac{M}{Ah} \bullet \frac{1}{nd - n(n-1)t} \tag{7}$$

where 'a' is the C–C bond length (0.144 nm) in a nanotube, which is slightly larger than that in graphite (0.142 nm) [30]. Each number of hexagons contributes two carbon atoms towards the mass of a tube.

2.4. Tortuosity evaluation method of VACNTs

During the growth of VACNT arrays, individual CNTs tend to form bundles that follow curved, non-linear trajectories rather than growing along perfectly straight paths [3,22,31,32]. As a result, the actual length of the CNT array is typically greater than the measured height of the VACNT array, as illustrated in Fig. 2. To estimate the ratio between the array height h and the average length l of these bundled CNTs, a custom Fourier component analysis algorithm is applied to cross-sectional SEM images of the VACNT structures.

This algorithm analyses the frequency components of the SEM images to assess the orientation distribution of the CNT arrays. It is modified from the directionality plugin from FIJI (ImageJ), which has been effectively employed in similar structural analysis contexts. The image processing workflow begins with Gaussian filtering to reduce noise and smooth the image, followed by directional normalisation to eliminate horizontal striping artefacts introduced by pixel-wise sampling in SEM acquisition. Next, a Fourier Transform of the pre-processed image is computed. A series of directional filters is then generated in the frequency domain. These filters, each corresponding to a specific orientation, are applied to the power spectrum of the Fourier Transform. The output provides the relative strength of CNT array alignment along each direction, enabling a quantitative assessment of orientation and an estimation of the average array length relative to the array height.

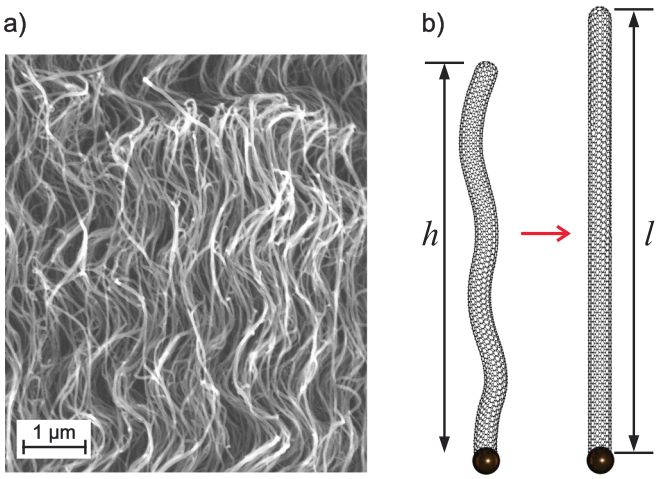

Fig. 2. CNT Tortuosity. (a) cross-sectional SEM image of a VACNT array and (b) illustration of comparison between measured height and real length of a CNT.

3. Results and discussion

3.1. Dependence of VACNT array structures on Fe catalyst film thickness

3.1.1. Catalyst particle size and distribution

The morphological properties of Fe catalyst nanoparticles were systematically investigated using AFM, which were analysed on 0.5 × 0.5 μm^2 regions of the nanoparticles (Fig. 3a). After the e-beam physical vapour deposition of Fe films, the catalyst nanoparticles were formed by subjecting the Fe films to the CVD growth cycle for VACNT synthesis without exposure to a carbon source to prevent CNT growth. This approach allowed for the precise characterisation of the catalyst nanoparticles. The AFM images were processed using custom code (in the supplement) for image segmentation and analysis(Fig. 3b-d).

The particle density exhibits a marked decrease as the initial catalyst thickness increases. The highest particle density was observed at 0.8 nm (1948 ± 140 μm^{-1}), with a progressive decline to 1048 ± 148 μm^{-1} at 2.0 nm catalyst thickness (Fig. 3b). This trend suggests that increasing catalyst film thickness leads to coalescence and a reduction in the number of discrete catalyst nanoparticles. A clear trend of increasing particle size was observed with increasing catalyst thickness (Fig. S3a). The mean particle diameter increased from 13.8 ± 4.8 nm at 0.8 nm to 20.2 ± 9.1 nm at 2.0 nm (Fig. 3c). This increase is accompanied by a growing standard deviation, indicating greater particle size heterogeneity at larger catalyst thicknesses, which is further illustrated in Fig. S3. Particle height (4.7–5.1 nm) remained relatively consistent for catalyst

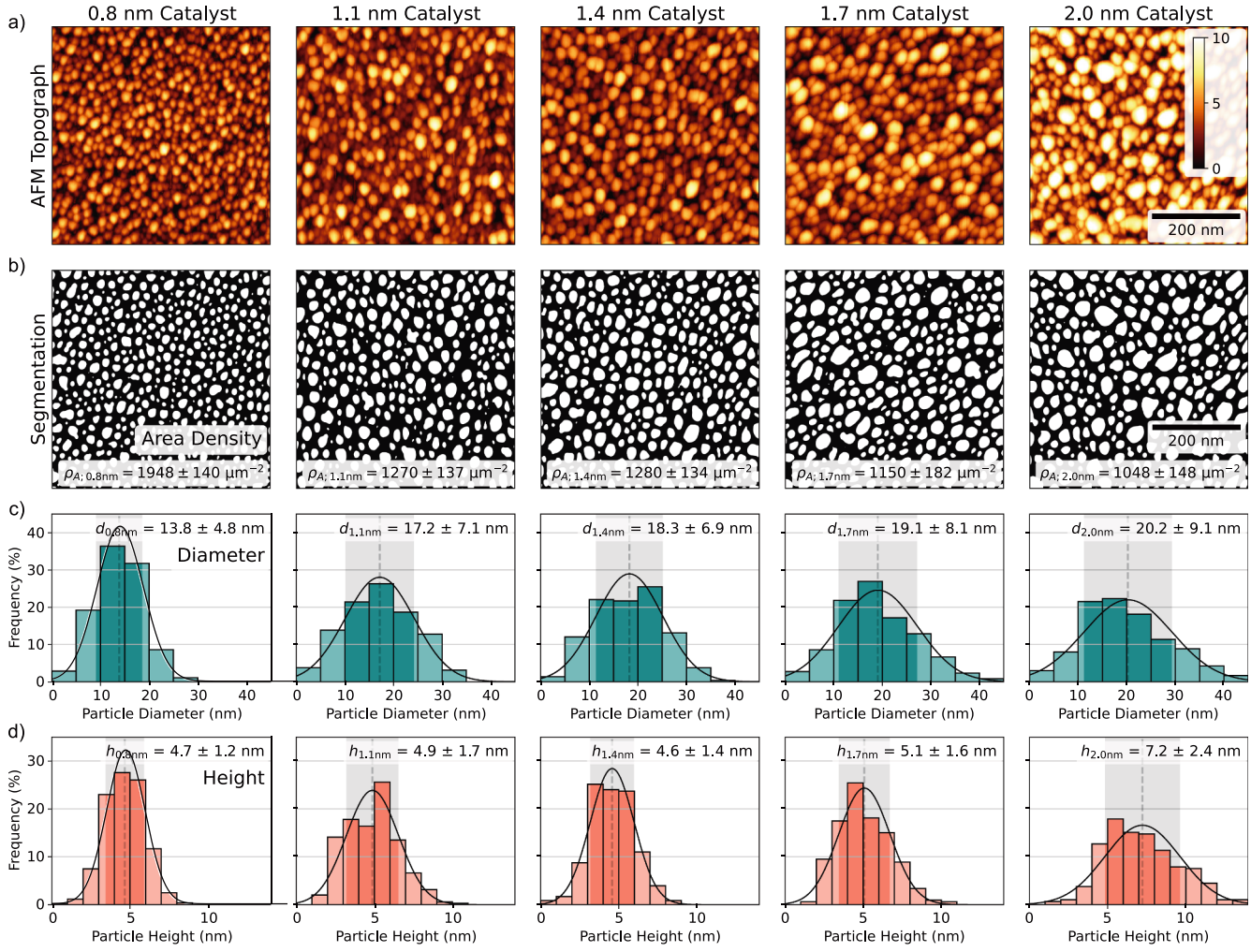

Fig. 3. Comprehensive imaging and statistical analysis of Fe catalyst nanoparticles. (a) original AFM images, (b) segmented nanoparticle images, (c) diameter distribution histograms, (d) height distribution histograms for different catalyst thicknesses (0.8, 1.1, 1.4, 1.7, and 2.0 nm).

thicknesses between 0.8 and 1.7 nm. However, a significant increase in height was observed at 2.0 nm (7.2 ± 2.4 nm) (Fig. 3d), suggesting a qualitative change in particle morphology at this thickness. The original AFM images and their segmented counterparts in Figs. 3a and 3b visually confirm these morphological changes; the size and height variations are comprehensively depicted in the size and height distribution histograms of Fig. 3(c, d), offering insight into the structural evolution of catalyst nanoparticles as a function of initial catalyst film thickness.

It is evident that the initial Fe film thickness strongly governs the catalyst particle morphology, which has been further confirmed by SEM images (as shown in Fig. S4). Thinner films yield dense, uniform nanoparticles, whereas thicker films lead to coalescence, resulting in reduced particle density and increased size heterogeneity. These results underscore film thickness as a key lever for tuning catalyst properties in CVD processes.

3.1.2. Diameter and walls of VACNTs

The diameter and wall number of CNTs play critical roles in determining their collective properties, such as electrical and thermal conductivity [33–36]. The size of the catalyst nanoparticles strongly influences both and is thus governed by the initial thickness of the catalyst film [37,38].

The diameter and walls of CNTs have been collected by the TEM (Fig. S5); typical TEM images of multi-walled CNTs are shown in Fig. 4. There is a weak correlation of wall number and CNT thickness; we can clearly distinguish different walls. Figs. 5(a) and (b) present the distribution of CNT diameters and wall numbers. The observed skewness toward a specific wall number is expected, as the catalyst film is uniformly deposited on the substrate, resulting in catalyst particles of relatively consistent size after agglomeration during the annealing phase. A similar distribution trend is observed for CNT diameters, which can be attributed to the uniformity of catalyst particle sizes, leading to a frequent occurrence of CNTs with a specific number of walls. Given the positive correlation between wall number and diameter, both distributions exhibit a comparable right-skewed shape, with a prominent peak around 9 nm in diameter and a skewed range between 7 and 10 nm.

As the Fe catalyst thickness increases, both the diameter and wall number distributions exhibit greater variance, suggesting a broader distribution of catalyst particle sizes. In contrast, the average diameters display an apparent linear increase (Fig. 5c). This observation aligns with AFM measurements of Fe nanoparticles, which show less uniformity at higher film thicknesses. Extending the annealing time beyond the standard five minutes would likely allow further coalescence of catalyst particles, potentially leading to more uniform particle sizes and narrower CNT diameter distributions [39].

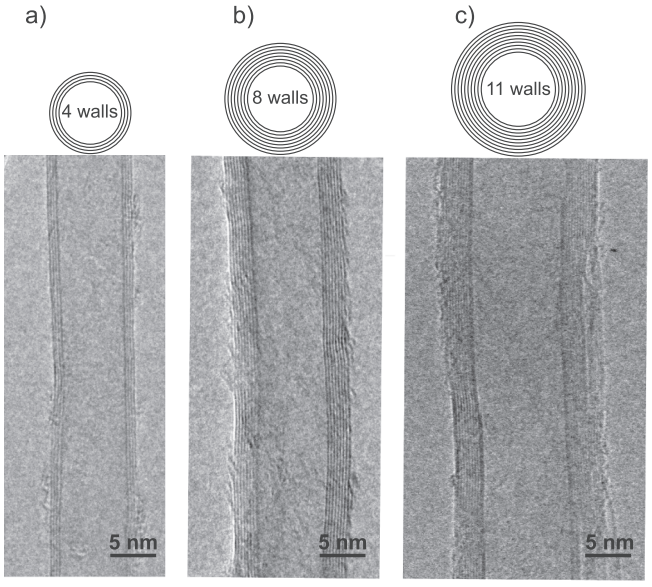

Fig. 4. High-resolution TEM images of (a) 4-walled, (b) 8-walled, and (c) 11-walled CNT.

3.1.3. Density of VACNT arrays

The density of VACNT arrays is a key metric for evaluating their quality across various applications. The average mass density and areal density can be calculated using Eqs. (1) and (7), respectively, based on averaged measurements of diameter, wall number, height, and weight, as shown in Fig. 5(d). The highest areal density (~2×10^{10} cm^2) is achieved at a Fe catalyst thickness of 1.1 nm. In contrast, the highest average mass density (~19 mg/cm^3) is observed at a thickness of 2.0 nm, despite this condition yielding lower areal density and shorter CNT height. This disparity is attributed to individual CNTs having larger diameters and more walls, resulting in a greater mass.

Thicker Fe films result in larger catalyst particles during the annealing process. This leads to the formation of CNTs with increased diameter and wall number, ultimately raising the mass of individual nanotubes and contributing to a higher overall forest mass density even when the areal density is relatively low. Conversely, the lowest areal density (~1.2×10^{10} cm^2) is observed at both the lowest (0.8 nm) and higher (1.7 nm) Fe thicknesses. This trend differs slightly from the previous research [39], although their work also indicates that increasing Fe thickness beyond 1.1 nm tends to reduce areal density. Therefore, 1.1 nm appears to be an optimal catalyst thickness, providing the highest areal density while maintaining a favourable mass density.

When comparing the average CNT areal density to the density of catalyst nanoparticles, it becomes evident that only a small fraction (less than 10 %) of the catalyst particles actively nucleate CNT growth. This finding is consistent with prior studies [26], which suggest that factors such as growth temperature and local chemical environment significantly influence catalyst activation and CNT nucleation.

3.2. Dynamic density change along VACNT array height

The growth of VACNT arrays is inherently non-uniform, and their density evolves dynamically over time. In this study, CNT arrays were grown for three different durations (30, 60, and 90 min) under strictly identical conditions, except for the growth time. This *ex-situ* approach enables the simplified observation of time-dependent changes in VACNT density. As illustrated in Fig. 6, the mass density varies along the height of the array.

In Fig. 6(a), the growth process can be divided into three phases. Phases 1 and 2 exhibit nearly identical growth rates across all Fe catalyst thicknesses, while Phase 3 shows a significant decline in growth rate. For Fe thicknesses of 0.8, 1.1, and 1.4 nm, the CNT growth rate decreases by approximately 30 % in Phase 3. For thicker catalyst layers (1.7 and 2.0 nm), the reduction exceeds 50 %. Fig. 6(b) shows corresponding trends in weight gain, which reflect changes in mass density. Phase 1 yields the most significant mass gain, indicating the highest mass density, except for the 0.8 nm Fe thickness. In Phase 2, mass density consistently declines, while in Phase 3, it slightly recovers for most samples, except for 1.1 nm, which continues to decrease. This behaviour may be attributed to increased tortuosity or buckling of CNTs during the later stages of growth, which will be discussed in Section 3.3.

Interestingly, while the 1.4 nm Fe thickness exhibits the highest growth rate, it does not significantly outperform the 0.8, 1.1, or even 1.7 nm thicknesses. Nevertheless, it results in the most significant weight gain, suggesting superior mass accumulation. The 2.0 nm Fe thickness demonstrates the slowest growth and lowest mass gain.

From a growth efficiency standpoint, both 1.1 and 1.4 nm Fe thicknesses appear optimal for achieving high-density, mm-tall scale VACNTs. For applications prioritising mass density (i.e., more hexagonal carbon lattices at a fixed CNT height), thicker catalyst layers may be preferable despite slower vertical growth.

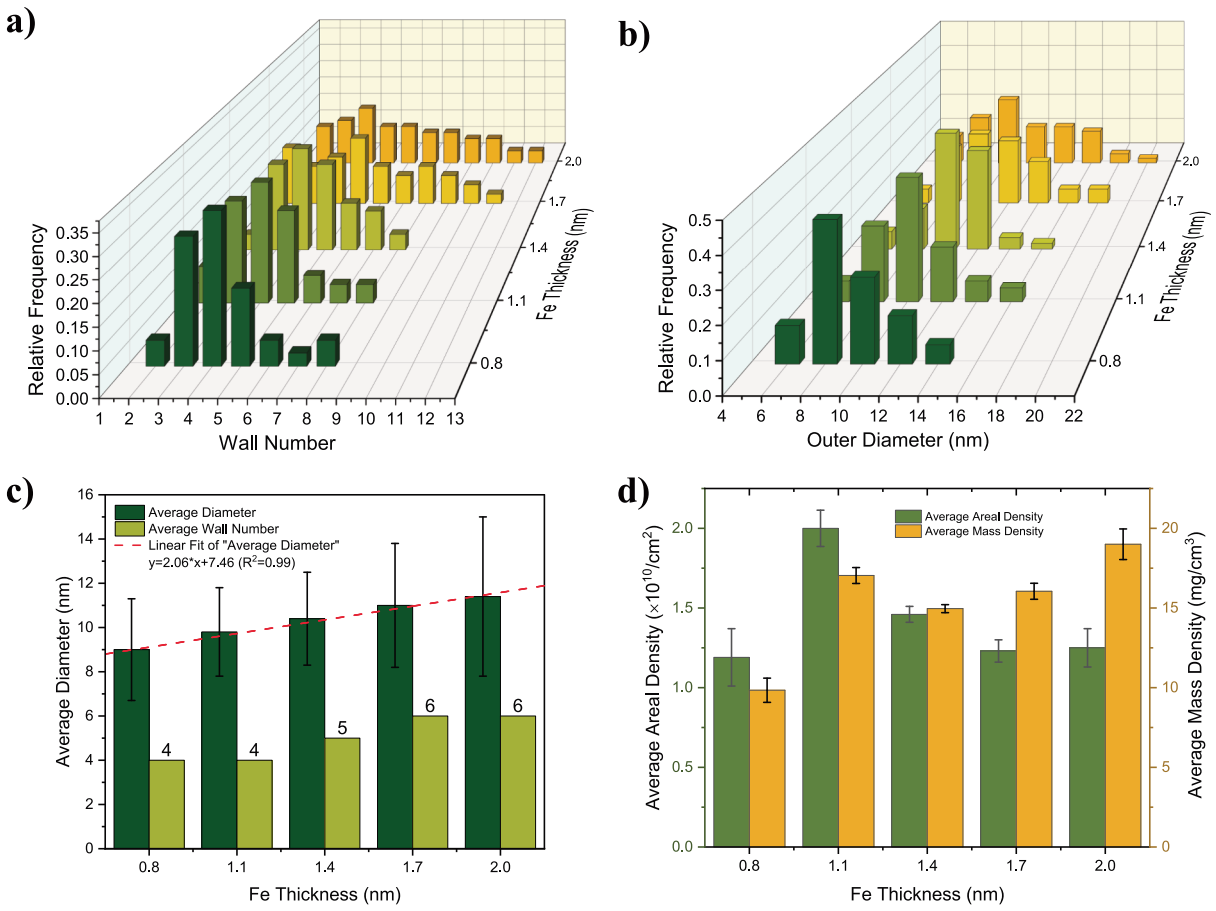

Fig. 5. Distribution histograms of (a) the diameter and (b) wall number in CNT arrays grown from different Fe thicknesses, (c) the relationship of Fe thickness and average diameter or the number of walls of CNTs, and (d) Average areal density (green histograms) and mass density (yellow histograms) at different Fe film thicknesses.

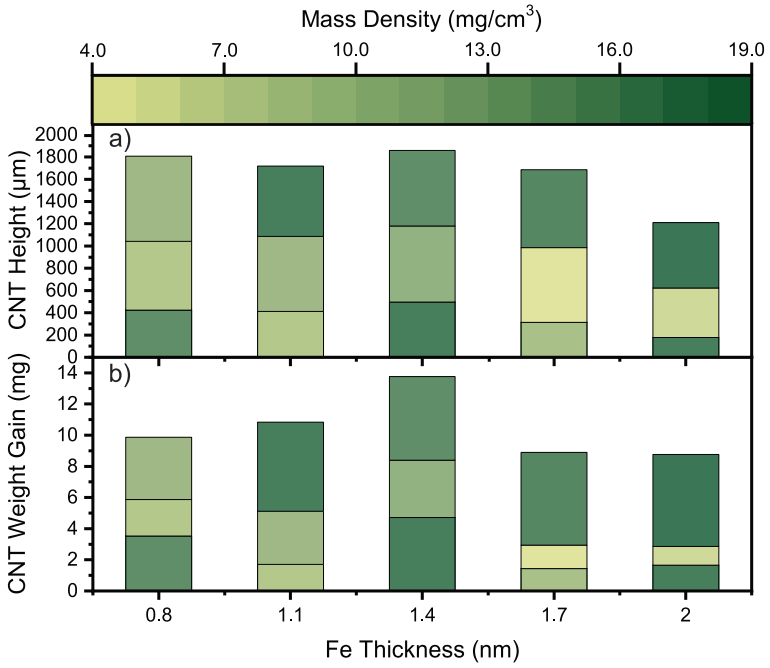

Fig. 6. Density map along with (a) CNT array length and (b) CNT array weight gain at different Fe thicknesses. The entire growth period is divided into three phases, as shown by the three blocks in the density map from top to bottom of one column, which represent three successive growth phases with the same time interval (Phase 1: 0–30 min, Phase 2: 30–60 min, Phase 3: 60–90 min).

By comparing Fig. 5(c,d) (areal/mass density) and Fig. 7 (temporal density evolution), it can be inferred that, within a narrow catalyst thickness range, lower CNT growth rates tend to correlate with higher mass densities. This observation is consistent with prior findings that the overall carbon mass yield remains stable over time [26]. Hence, tracking the evolution of VACNT mass density offers a more accurate metric of reaction kinetics, as it directly reflects the carbon incorporation rate into the growing CNT population.

3.3. Growth tortuosity of VACNT arrays

Although often overlooked in prior studies, growth tortuosity plays a critical role in shaping the structural properties of mm-tall VACNT arrays. In this work, each CNT array was vertically segmented into several equal slices using SEM. SEM imaging revealed distinct alignment behaviours at different growth stages of the CNTs.

In the early growth phase, corresponding to the top of the CNT array, initially grown nanotubes appear entangled due to the lack of structural self-support. Following a brief period of steady growth, the density of the CNT array gradually declines, driven by the cumulative deactivation of catalyst nanoparticles, ultimately leading to self-termination of growth. At its maximum, the density stabilises over a limited section (less than 20 % of the total height) of the array. In the later stages of growth, near the base of the array, CNTs may either maintain alignment or become entangled, depending on the residual active growth time [40]. In this work, VACNTs grown for more than 60 min often exhibit sparse and disordered structures near the bottom, primarily due to a substantial reduction in the number of active catalyst nanoparticles. Notably, the central region, which accounts for approximately 30 % of the array height, tends to exhibit the best alignment across the forest.

The ratio between CNT length and array height reveals that the measured height significantly underestimates the actual CNT length in mm-tall arrays. Consequently, an accurate assessment of areal density requires correction by evaluating tortuosity within each segmented slice of the array. The maximum observed length-to-height ratio can reach up to 20 % at the bottom of the VACNT array (Fig. 7a).

Fig. 7a presents SEM micrographs of VACNT sidewalls at different heights and the corresponding tortuosity, showcasing this variation in alignment. These images are used to generate histograms of directional densities, which capture the predominant orientations of CNT bundles. From this analysis, the actual bundle length relative to the array height can be estimated.

With prolonged growth time, the VACNT array becomes progressively sparser and more entangled due to the decline in active catalyst nanoparticle population. Our findings suggest that a specific catalyst thickness (1.1 nm) results in a denser and more aligned VACNT array than other tested thicknesses (details on additional thicknesses evaluated are presented in Section 3.1.3). When CNT arrays grow too sparse to support their own weight, failing to maintain a self-supporting morphology, they may undergo collective buckling, as illustrated in Fig. S5. Interestingly, however, continuous growth can sometimes resume even under constant reaction conditions. This suggests that some catalyst nanoparticles may be reactivated during growth, although the underlying mechanism requires further investigation.

A particularly unusual phenomenon observed in our experiments is that specific CNT arrays exhibit buckling once their length exceeds ~1 mm but subsequently return to an aligned state and continue growing, as shown in Fig. S6. This transitional morphology often coincides with unstable conditions in the TCVD system. We hypothesise that such fluctuations may trigger the activation of new catalyst nanoparticles, though conclusive evidence remains to be established.

3.4. Growth mode transition observation

Notably, TEM images in Fig. 7(b) show that some Fe nanoparticles were observed to be fully encapsulated by graphite layers with the same number of walls as the CNT main body. The encapsulated Fe nanoparticles exhibited a water-drop morphology, suggesting a phase change in the catalyst even during the initial stages of CNT growth. It is worth noting that this encapsulation was only observed at a thickness of 2.0 nm, but not at other thicknesses.

The growth mode may transition between base growth and tip growth, depending on the adhesion strength of the catalyst particles to the substrate [41–43]. However, the precise mechanism underlying catalyst detachment remains unclear [1]. One plausible explanation for encapsulation is that high-temperature conditions destabilise the metal nanoparticles due to surface distortions, leading to detachment and the formation of a tear-like droplet at the growing CNT tip [37]. Interestingly, no antiparticles were observed in the mid-sections of the CNTs in this study [44,45].

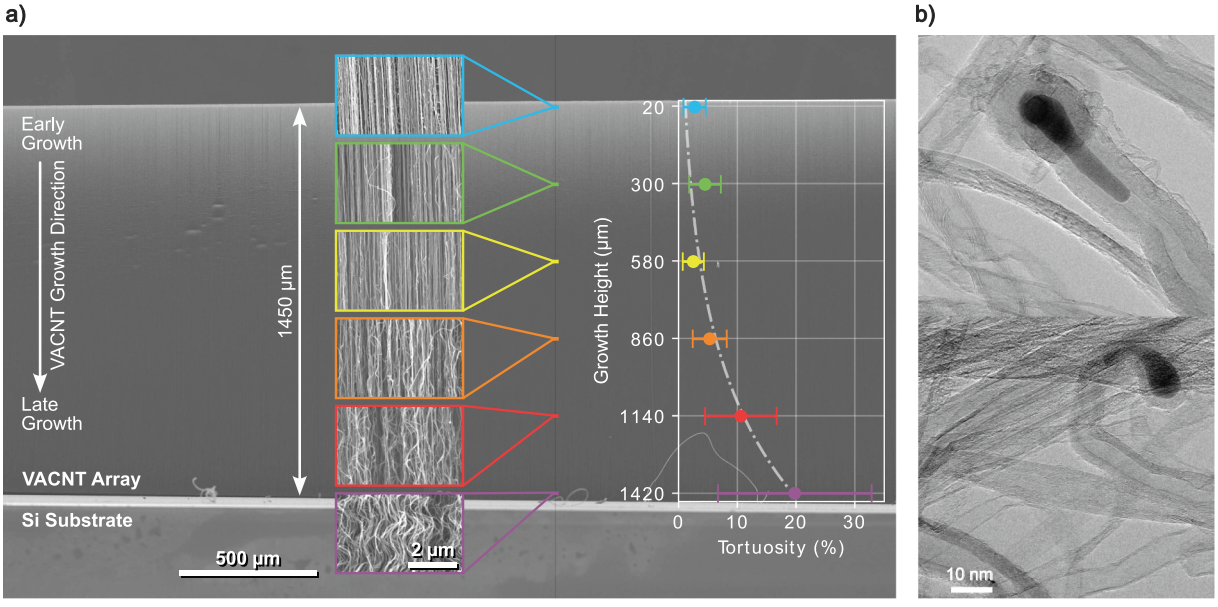

Fig. 7. (a) SEM images of the cross-section profile of as-grown VACNTs and the close-up views of as-grown VACNTs in different positions corresponding to different tortuosity. (b) Representative TEM images of CNTs with encapsulated Fe nanoparticles at the ends.

Nevertheless, our observations suggest that a Fe catalyst film thickness of ~1.7 nm may represent a critical threshold for growth mode transition. A potential explanation is that smaller nanoparticles exhibit strong substrate adhesion, favouring base growth, where the catalyst remains anchored while CNTs elongate upward. In contrast, larger Fe nanoparticles forming at a thickness of ~2.0 nm are more susceptible to detachment due to weaker substrate interactions and enhanced capillary forces. The detached nanoparticles become encapsulated at the CNT tip, and progressive carbon deposition eventually leads to the complete enclosure of nanoparticles within the CNT walls. However, further investigation is needed to fully elucidate this behaviour, though such analysis lies beyond the scope of this work.

4. Conclusion

A comprehensive analysis of mm-tall VACNT arrays was conducted using the proposed characterisation methods. Fe film thickness critically controls catalyst nanoparticle size and distribution, while thicker films form larger, heterogeneous ensembles. Carefully varying Fe thickness enables fine control of nanotube diameter and wall number without compromising areal density. Optimal catalyst thickness of ~1.1 nm achieves peak packing density by balancing particle density and size. Mass density analysis combining mass-gain measurements with TEM and SEM imaging reveals vertical density gradients, providing a rapid, instrumentation-light approach for monitoring growth dynamics. However, SEM-measured height underestimates actual CNT length due to bundle tortuosity, causing up to 20 % density overestimation. Detailed SEM analysis shows alignment quality degrades with height, with initial growth stages exhibiting high vertical alignment and later stages showing increased curvature. Fourier component analysis of cross-sectional SEM images corrects this underestimation, enabling accurate density calculations and deeper insight into growth evolution.

Our research helps bridge the gap between measurements of individual nanostructures and bulk material properties, providing simple guidance for quickly tailoring CNT properties. This rapid characterisation protocol directly addresses the critical bottleneck in VACNT research and development: the slow optimisation cycle. By delivering reliable density and morphological data within hours, it enables an agile, data-driven optimisation. This transforms VACNT development from an empirical art into a rapid, closed-loop system, drastically accelerating the industrial translation of VACNT-based applications.

Future studies should investigate the kinetics of catalyst deactivation and reactivation during extended growth, examine the impact of alternative carbon precursors on tortuosity, and integrate real-time optical or electrical diagnostics to further refine process control. Investigating catalyst-support interactions and extending this methodology to other substrate materials will broaden the applicability of these findings for the scalable integration of CNT-based devices. The growth mode transition resulting from a change in catalyst thickness is also worthy of future investigation.

CRediT authorship contribution statement

Xinghai Zhao: Writing – review & editing, Writing – original draft, Visualization, Methodology, Investigation, Formal analysis, Conceptualization. **Johannes Eduard Stubbe:** Writing – review & editing, Writing – original draft, Investigation. **Jin Chuen Kenneth Ho:** Writing – review & editing, Investigation, Formal analysis. **Putu Andhita Dananjaya:** Investigation. **Wen Siang Lew:** Investigation. **Philippe Coquet:** Resources, Supervision. **Beng Kang Tay:** Validation, Resources, Supervision.

Declaration of competing interest

The authors declare that they have no known competing financial interests or personal relationships that could have appeared to influence the work reported in this paper.

Acknowledgments

The authors would like to acknowledge Prof. H.T. Teo for providing the TCVD system used in this work and the Facility for Analysis, Characterisation, Testing and Simulation (FACTS), Nanyang Technological University, for the use of their TEM facility. The authors also thank Dr. J. P. Zou, Dr. K. Liang and Dr. C.W. Tan for their support. The authors would like to acknowledge funding support from the National Research Foundation, Singapore and Infocomm Media Development Authority under its Future Communications Research & Development Programme (FCP-CNRS-RG-2022-022(REQ0396559)). X. Zhao would like to acknowledge the Wallenberg-NTU Research Fellowship.

Appendix A. Supplementary data

Supplementary data to this article can be found online at https://doi.org/10.1016/j.apsusc.2025.165504.

Data availability

Data will be made available on request.

References

[1] A. Hoque, C.P. Nawarathne, N.T. Alvarez, Vertically aligned carbon nanotubes from premade binary metal oxide nanoparticles on bare SiO2, Carbon 235 (2025) 120086.
[2] D. Zhi-jun, S. Bing, Z. Hui, Y. Guan-ming, L. Bao-liu, G. Jian-guang, L. Xuan-ke, C. Ye, Z. Jiang, A review of aligned carbon nanotube arrays and carbon/carbon composites: fabrication, thermal conduction properties and applications in thermal management, New Carbon Mater. 36 (5) (2021) 873.
[3] X. Zhao, D. Chu, X. Zhang, C. Gao, Y. He, W. Bai, Growth and characterization of carbon nanotubes and study of modified carbon fiber—A review, Diam. Relat. Mater. 147 (2024) 111308.
[4] M. Ahmad, S.R.P. Silva, Low temperature growth of carbon nanotubes – a review, Carbon 158 (2020) 24–44.
[5] C. Chatelet, U. Forestier-Colleoni, P. Banet, J. Descarpentries, T.G. de Monsabert, F. Nassoy, C. Reynaud, M. Pinault, Vertically aligned carbon nanotubes on aluminum foils from biosourced precursors: Application to energy storage, Carbon Trends 19 (2025) 100450.
[6] L. Fedina, D. Sheglov, O. Semenova, S. Rodyakin, D. Nasimov, N. Kurus, A. Gutakovskii, V. Golyashov, I. Chistokhin, A. Jaroshevich, M. Dem'yanenko, V. Gaisler, S. Sitnikov, D. Rogilo, A. Dudin, A. Pavlov, A. Latyshev, Effect of CF4 plasma treatment on the THz radiation absorption of vertically aligned carbon nanotubes, Appl. Surf. Sci. 689 (2025) 162537.
[7] H. Grzywacz, D.M. Jarząbek, P. Pietrzyk-Thel, K. Stępniak, A. Roszkiewicz, W. J. Dera, Low-content MWCNTs–PVDF composites for nanoscale actuation: Crystalline tailoring and in-situ electro-mechanical analysis using hybrid AFM–Sawyer-Tower system, Carbon 245 (2025) 120738.
[8] B.Q. Wei, R. Vajtai, P.M. Ajayan, Reliability and current carrying capacity of carbon nanotubes, Appl. Phys. Lett. 79 (8) (2001) 1172–1174.
[9] H. Du, P. Jiang, D. Xiao, W. Wang, Y. Tang, X. Yang, L. Sun, Interface engineering of TiC-functionalized carbon nanotubes for 3D optoelectronics, Carbon 235 (2025) 120087.
[10] L. Lum, D. Tan, C.W. Tan, B.K. Tay, Electromagnetic crosstalk isolation with transferred vertically aligned carbon nanotube arrays through thermocompression bonding, Carbon 221 (2024) 118943.
[11] K. Nishita, T. Nakano, Y. Shimizu, M. Nagata, S. Yanai, N. Shirai, T. Omatsu, Y. Inoue, Impact of dynamic density decay of growing carbon nanotube forests on electrical resistivity, Carbon 218 (2024) 118749.
[12] G. Zhong, J.H. Warner, M. Fouquet, A.W. Robertson, B. Chen, J. Robertson, Growth of ultrahigh density single-walled carbon nanotube forests by improved catalyst design, ACS Nano 6 (4) (2012) 2893–2903.
[13] G. Chen, B. Dodson, D.M. Hedges, S.C. Steffensen, J.N. Harb, C. Puleo, C. Galligan, J. Ashe, R.R. Vanfleet, R.C. Davis, Fabrication of high aspect ratio millimeter-tall free-standing carbon nanotube-based microelectrode arrays, ACS Biomater Sci. Eng. 4 (5) (2018) 1900–1907.
[14] X. Zhao, R. Jiang, C.W. Tan, L.L. Yuxiang, P. Coquet, D. Baillargeat, B.K. Tay, Investigation of Vertically Aligned Carbon Nanotube Arrays as Building Blocks for mm-Wave Waveguide Devices, in: 2023 Asia-Pacific Microwave Conference (APMC), IEEE, 2023, pp. 754–756.
[15] Q. Liu, X. Shi, Q. Jiang, R. Li, S. Zhong, R. Zhang, Growth mechanism and kinetics of vertically aligned carbon nanotube arrays, EcoMat 3 (4) (2021) e12118.
[16] C. Xu, Y. Li, L. Wang, L. Shi, Z. Dai, Experimental and first-principles study on the interfacial interactions between vertically aligned carbon nanotubes and growth

substrates: prospects for better substrate adhesion, Diam. Relat. Mater. 133 (2023) 109734.
[17] B. Zhao, D.N. Futaba, S. Yasuda, M. Akoshima, T. Yamada, K. Hata, Exploring advantages of diverse carbon nanotube forests with tailored structures synthesized by supergrowth from engineered catalysts, ACS Nano 3 (1) (2009) 108–114.
[18] B. Goh, K.J. Kim, E.S. Kim, S.H. Kim, J. Choi, Outer diameter Curvature effects in Multi-Walled carbon nanotubes on the twistron energy harvester, Appl. Surf. Sci. 561 (2021) 150075.
[19] K. Hayashi, T. Nakano, Y. Inoue, Enhancing thermal conduction properties of vertically aligned CNT forests by reducing interfacial thermal resistance using an aluminum interlayer, Carbon 238 (2025) 120256.
[20] B. Xu, R. Chen, J. Zhou, J. Liang, Recent progress and challenges regarding carbon nanotube on-chip interconnects, Micromachines 13 (7) (2022) 1148.
[21] Y. Zhang, G. Zou, S.K. Doorn, H. Htoon, L. Stan, M.E. Hawley, C.J. Sheehan, Y. Zhu, Q. Jia, Tailoring the morphology of carbon nanotube arrays: from spinnable forests to undulating foams, ACS Nano 3 (8) (2009) 2157–2162.
[22] K. Tabata, Y. Kono, R. Goto, Y. Abe, T. Nakano, H. Sugime, Y. Inoue, Catalyst dynamics in the growth of high-density cnt forests; fine control of the mass density of forest by colloidal catalyst nanoparticles, J. Phys. Chem. C 126 (48) (2022) 20448–20455.
[23] Z. Lao, X. Liu, F. Li, Y. Chen, K. Yang, L. Chen, L. Jiang, K. Mai, Z. Zhang, Areal density control of liquid-supported carbon nanotube thin films, Langmuir 38 (48) (2022) 14760–14767.
[24] S. Esconjauregui, R. Xie, M. Fouquet, R. Cartwright, D. Hardeman, J. Yang, J. Robertson, Measurement of area density of vertically aligned carbon nanotube forests by the weight-gain method, J. Appl. Phys. 113 (14) (2013).
[25] H. Bi, K. Yin, X. Xie, Y. Zhou, N. Wan, F. Xu, F. Banhart, L. Sun, R.S. Ruoff, Low temperature casting of graphene with high compressive strength, Adv. Mater. 24 (37) (2012) 5124–5129.
[26] M. Bedewy, E.R. Meshot, M.J. Reinker, A.J. Hart, Population growth dynamics of carbon nanotubes, ACS Nano 5 (11) (2011) 8974–8989.
[27] P. Sharma, V. Pavelyev, S. Kumar, P. Mishra, S.S. Islam, N. Tripathi, Analysis on the synthesis of vertically aligned carbon nanotubes: growth mechanism and techniques, J. Mater. Sci. Mater. Electron. 31 (6) (2020) 4399–4443.
[28] R. Waelder, C. Park, A. Sloan, J. Carpena-Núñez, J. Yoho, S. Gorsse, R. Rao, B. Maruyama, Improved understanding of carbon nanotube growth via autonomous jump regression targeting of catalyst activity, Carbon 228 (2024) 119356.
[29] A. Peigney, C. Laurent, E. Flahaut, R.R. Bacsa, A. Rousset, Specific surface area of carbon nanotubes and bundles of carbon nanotubes, Carbon 39 (4) (2001) 507–514.
[30] G.F. Zhong, T. Iwasaki, H. Kawarada, Semi-quantitative study on the fabrication of densely packed and vertically aligned single-walled carbon nanotubes, Carbon 44 (10) (2006) 2009–2014.
[31] A.B. Al Tahhan, M. Alkhedher, A.H.I. Mourad, M. Ramadan, M.A. Shehadeh, Molecular Dynamics study on buckling behavior of vertically aligned carbon nanotube (VACNT) bundles with characterized waviness, Comput. Mater. Sci. 228 (2023).
[32] B.K. Wittmaack, A.N. Volkov, L.V. Zhigilei, Phase transformation as the mechanism of mechanical deformation of vertically aligned carbon nanotube arrays: Insights from mesoscopic modeling, Carbon 143 (2019) 587–597.
[33] A. Nieuwoudt, Y. Massoud, Evaluating the impact of resistance in carbon nanotube bundles for VLSI interconnect using diameter-dependent modeling techniques, IEEE Trans. Electron Devices 53 (10) (2006) 2460–2466.
[34] M.B. Jakubinek, M.A. White, G. Li, C. Jayasinghe, W. Cho, M.J. Schulz, V. Shanov, Thermal and electrical conductivity of tall, vertically aligned carbon nanotube arrays, Carbon 48 (13) (2010) 3947–3952.
[35] B. Xu, R. Chen, J. Zhou, J. Liang, A Modeling study on electrical and thermal behavior of CNT TSV for multilayer structure, IEEE Trans. Electron Devices 70 (9) (2023) 4779–4785.
[36] Z. Pápa, E. Kecsenovity, D. Fejes, J. Budai, Z. Toth, K. Hernadi, Height and diameter dependence of carbon nanotube forests on the porosity and thickness of catalytic layers, Appl. Surf. Sci. 428 (2018) 885–894.
[37] O.A. Nerushev, S. Dittmar, R.-E. Morjan, F. Rohmund, E.E.B. Campbell, Particle size dependence and model for iron-catalyzed growth of carbon nanotubes by thermal chemical vapor deposition, J. Appl. Phys. 93 (7) (2003) 4185–4190.
[38] L. Ci, R. Vajtai, P.M. Ajayan, Vertically aligned large-diameter double-walled carbon nanotube arrays having ultralow density, J. Phys. Chem. C 111 (26) (2007) 9077–9080.
[39] A. Rizzo, R. Rossi, M.A. Signore, E. Piscopiello, L. Capodieci, R. Pentassuglia, T. Dikonimos, R. Giorgi, Effect of Fe catalyst thickness and C_2H_2/H_2 flow rate ratio on the vertical alignment of carbon nanotubes grown by chemical vapour deposition, Diam. Relat. Mater. 17 (7) (2008) 1502–1505.
[40] O.T. Gul, A simple method to grow millimeters long vertically aligned carbon nanotube forests, Diam. Relat. Mater. 120 (2021) 108637.
[41] I.K. Song, W.J. Yu, Y.S. Cho, G.S. Choi, D. Kim, The determining factors for the growth mode of carbon nanotubes in the chemical vapourdeposition process, Nanotechnology 15 (10) (2004) S590.
[42] X. Chen, X. Pang, C. Fauteux-Lefebvre, The base versus tip growth mode of carbon nanotubes by catalytic hydrocarbon cracking: Review, challenges and opportunities, Carbon Trends 12 (2023) 100273.
[43] J. Dijon, P.D. Szkutnik, A. Fournier, T. Goislard de Monsabert, H. Okuno, E. Quesnel, V. Muffato, E. De Vito, N. Bendiab, A. Bogner, N. Bernier, How to switch from a tip to base growth mechanism in carbon nanotube growth by catalytic chemical vapour deposition, Carbon 48 (13) (2010) 3953–3963.
[44] C.P. Deck, G.S. McKee, K.S. Vecchio, Synthesis optimization and characterization of multiwalled carbon nanotubes, J. Electron. Mater. 35 (2006) 211–223.
[45] J. Bora, B. Basumatary, S. Podder, D. Gogoi, B. Sharma, P. Bhagowati, B. Choudhury, D.S. Patil, A.R. Pal, A substrate constituent Na-catalyzed growth of carbon nanotubes on glass substrate by atmospheric pressure PECVD, Appl. Surf. Sci. 648 (2024) 158988.